Acta Biomaterialia 146 (2022) 259–273

Contents lists available at ScienceDirect

Acta Biomaterialia

journal homepage: www.elsevier.com/locate/actbio

Full length article

Comprehensive experimental assessments of rheological models' performance in elastography of soft tissues

Sedigheh S. Poul[a], Juvenal Ormachea[b], Gary R. Ge[c], Kevin J. Parker[b,*]

[a] Department of Mechanical Engineering, University of Rochester, Rochester, NY 14627, USA
[b] Department of Electrical and Computer Engineering, University of Rochester, Rochester, NY 14627, USA
[c] Institute of Optics, University of Rochester, Rochester, NY 14627, USA

ARTICLE INFO

Article history:
Received 8 February 2022
Revised 26 April 2022
Accepted 28 April 2022
Available online 5 May 2022

Keywords:
Elastography
Rheological model
Shear wave speed dispersion
Stress relaxation
Viscoelastic soft tissues

ABSTRACT

Elastography researchers have utilized several rheological models to characterize soft tissue viscoelasticity over the past thirty years. Due to the frequency-dependent behavior of viscoelastic parameters as well as the different techniques and frequencies employed in various studies of soft tissues, rheological models have value in standardizing disparate techniques via explicit mathematical representations. However, the important question remains: which of the several available models should be considered for widespread adoption within a theoretical framework? We address this by evaluating the performance of three well established rheological models to characterize *ex vivo* bovine liver tissues: the Kelvin-Voigt (KV) model as a 2-parameter model, and the standard linear solid (SLS) and Kelvin-Voigt fractional derivative (KVFD) models as 3-parameter models. The assessments were based on the analysis of time domain behavior (using stress relaxation tests) and frequency domain behavior (by measuring shear wave speed (SWS) dispersion). SWS was measured over a wide range of frequency from 1 Hz to 1 kHz using three different tests: (i) harmonic shear tests using a rheometer, (ii) reverberant shear wave (RSW) ultrasound elastography scans, and (iii) RSW optical coherence elastography scans, with each test targeting a distinct frequency range. Our results demonstrated that the KVFD model produces the only mutually consistent rendering of time and frequency domain data for liver. Furthermore, it reduces to a 2-parameter model for liver (correspondingly to a 2-parameter "spring-pot" or power-law model for SWS dispersion) and provides the most accurate predictions of the material viscoelastic behavior in time (>98% accuracy) and frequency (>96% accuracy) domains.

Statement of Significance

Rheological models are applied in quantifying tissues viscoelastic properties. This study is unique in presenting comprehensive assessments of rheological models:

- We employed experimental data in both the frequency domain (shear wave speed (SWS) vs. frequency) and time domain (stress relaxation) to assess rheological models' performances.
- SWS were acquired over a wide frequency range, 1 Hz to 1 kHz, by three independent techniques.
- Using the frequency domain analysis, we evaluated how well each model can *predict* measured time domain behaviors (and vice versa).
- This presents wide-ranging experimental proofs as the most comprehensive study of its type in terms of the number of experiments, frequency range, and conjoined assessments of time and frequency domains behaviors, demonstrating the most appropriate rheological model for soft tissues.

* Corresponding author.
E-mail address: kevin.parker@rochester.edu (K.J. Parker).

https://doi.org/10.1016/j.actbio.2022.04.047
1742-7061/

1. Introduction

Shear wave elastography (SWE) enables quantitative measurements of mechanical properties of tissues which may serve as biomarkers for characterizing normal vs. diseased tissue. With the robust evolution of the field of elastography [1,2], the capability to measure viscoelastic properties of tissues are expanding. These properties include shear wave speed (SWS), shear wave attenuation (SWA), shear wave dispersion (SWD), elasticity, and viscosity. These parameters have been widely measured by several groups using a variety of techniques to characterize viscoelastic soft tissues such as liver [3–9], breast [10,11], prostate [12], kidney [13,14], brain [15,16], aortic tissues [17,18], etc. or to characterize tissue-mimicking phantoms [19–22] or for characterization of models of tissues by employing numerical methods [23–25].

Today more research and clinical groups can extract measurements from wider classes of tissues than ever before. Therefore, rheological models have renewed attention for predicting tissue behavior over a wide frequency/time range in the form of explicit mathematical representations and providing a common framework between different measurement techniques. However, this raises ever more urgently the question: can soft tissue viscoelastic measures be placed within a common rheological model, and if so *which* of the several models should be considered for widespread adoption? In a previous publication [26], this question was explored with a general review of available data from soft tissues in the literature over specific time and frequency ranges. These were examined in light of the most common linear and fractional models. Combined with a philosophical view related to Occam's razor (where the simplest solution is preferred), and Akaike's principle of parsimony [27], this survey recommended the abandonment of the widely used Kelvin-Voigt single relaxation time constant model in favor of a simple fractional derivative model.

Given the importance of a common theoretical framework for comparison of results between different studies and techniques, the subject of a consensus (or lack thereof) deserves further attention. Specifically, in this paper the most common types of time and frequency domain experiments are compared for compatibility with well-known rheological models. Any model that can accurately describe a variety of important experimental results, and can do so with only a few parameters, is objectively a strong candidate for consensus adoption. Conversely, any model that fails to describe the most common types of responses or that requires a larger number of parameters should be abandoned.

In this study, we investigated the performance of three most common and well-known rheological models from a comprehensive practical and experimental view. We employed three independent and experimental tests to obtain frequency domain data related to the dispersion of phase velocity, and an independent test in the time domain related to stress relaxation. The frequency domain dispersion behavior is studied over a wider frequency range (1 Hz – 1 kHz) than has been previously evaluated to the best of our knowledge. We also demonstrated the success or failure of models' best parameter fits from two directions: will the parameters obtained from fitting the frequency domain (phase velocity dispersion) data predict the time domain (stress relaxation) results? Alternatively, will parameters obtained from fitting the time domain data accurately predict the frequency domain results? These twin approaches are illustrated in Fig. 1.

These questions are important because it is common to curve-fit a few frequency domain measurements (over a limited bandwidth) to multiple models, without regard to the implication of these models for prediction of simple stress relaxation results. We believe this study is the most comprehensive study of its type in terms of the number of independent experimental techniques applied, the wide frequency range of tests, and the critical assessment of joint time and frequency domains behaviors.

2. Theory

2.1. Viscoelastic media

Viscoelasticity manifests itself in the material properties of a medium as being (i) complex (having real and imaginary components) and (ii) frequency-dependent, as opposed to an elastic medium in which the material properties are real and do not change over a frequency range. The viscous component introduces a dissipative (imaginary) behavior which is responsible for dispersion. Quantification of these properties *in vivo* could result in obtaining a biomarker to assess the tissue characteristics in normal and diseased states.

For a viscoelastic medium, shear wave propagation and the underlying complex wavenumber $\hat{k}(\omega)$ could relate to its complex shear modulus $\hat{G}(\omega)$ according to Eq. (1) in which ω and ρ are the radial frequency and the density, respectively. The complex shear modulus is related to complex Young's modulus $\hat{E}(\omega)$ by the Poisson's ratio ν according to Eq. (2). For soft tissues, ν is approximated as nearly incompressible ($\nu \sim 0.5$), and the equation is simplified [26]:

$$\hat{k}(\omega) = \frac{\omega}{\sqrt{\frac{\hat{G}(\omega)}{\rho}}} \tag{1}$$

$$\hat{G}(\omega) = \frac{\hat{E}(\omega)}{2(1+\nu)} \overset{(\nu \sim 0.5)}{\Rightarrow} \hat{G}(\omega) = \frac{\hat{E}(\omega)}{3} \tag{2}$$

Furthermore, the complex wavenumber incorporates information regarding SWS, $c_{ph}(\omega)$, (as a measure of stiffness) as well as shear wave attenuation $\alpha(\omega)$ (as a measure of loss) of the medium as shown in Eq. (3):

$$\hat{k}(\omega) = \frac{\omega}{c_{ph}(\omega)} - j\alpha(\omega) \tag{3}$$

Using equations (1) - (3), SWS as a function of frequency is obtained from the complex modulus ($\hat{E}(\omega) = \hat{E}_{stor} + j\hat{E}_{loss}$):

$$c_{ph}(\omega) = \sqrt{\frac{2}{3\rho}} \frac{\hat{E}(\omega)}{\sqrt{\left|\hat{E}(\omega)\right| + \hat{E}_{stor}}} = \sqrt{\frac{2}{3\rho}} \frac{\hat{E}_{stor}^2 + \hat{E}_{loss}^2}{\sqrt{\hat{E}_{stor}^2 + \hat{E}_{loss}^2} + \hat{E}_{stor}} \tag{4}$$

In which $\hat{E}_{stor}$ and $\hat{E}_{loss}$ are the storage and loss Young's moduli, respectively.

Another important characteristic of viscoelastic media is their stress relaxation (SR) behavior, which originates from their time-dependent behavior.

The stress relaxation behavior of a viscoelastic medium is characterized as a time-dependent decrease in stress when the medium is exposed to an *ideal* (sudden) step strain function. In practical experiments on the viscoelastic materials, applying this *ideal* strain cannot be physically implemented and a step strain is applied in two successive steps as shown in Eq. (5): first, a short linear ramp strain is applied until the desired strain level ε_0 is achieved during [0-T_0] time period. This is followed by the application of a constant strain ε_0 for the rest of the experiment. The latter is associated with the stress relaxation period in time [28].

$$\text{Ramp} - \text{and} - \text{hold strain}: \quad \varepsilon(t) = \begin{cases} \frac{\varepsilon_0}{T_0} t & t < T_0 \\ \varepsilon_0 & t \geq T_0 \end{cases} \tag{5}$$

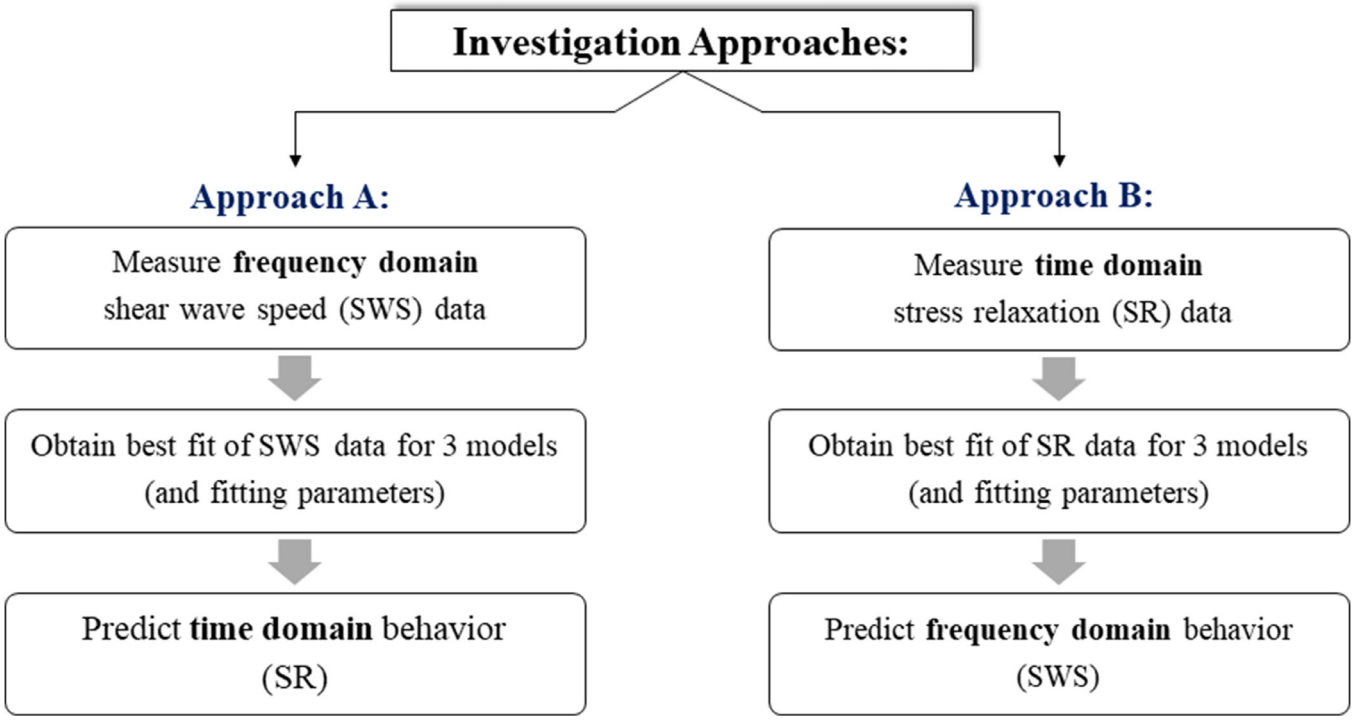

Fig. 1. The flowchart showing the summary of the two approaches for analyzing the three rheological models: Approach A: frequency domain analysis; Approach B: time domain analysis.

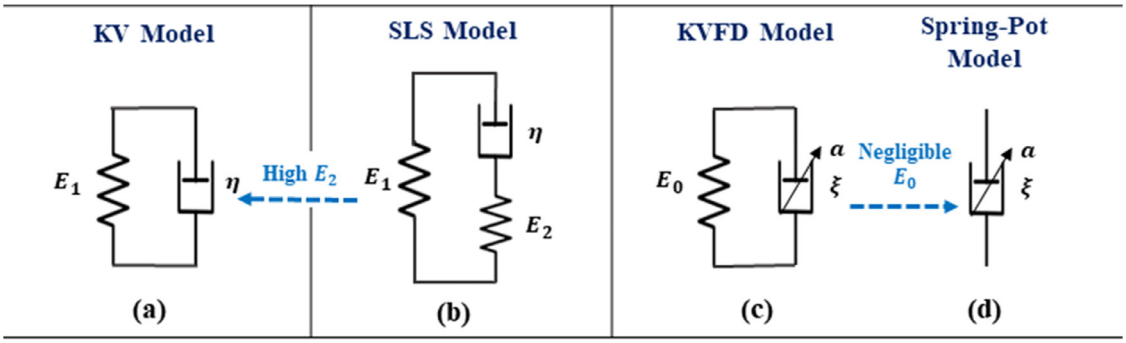

Fig. 2. Diagrams of rheological models: (a) KV model, (b) SLS model, (c) KVFD model, and (d) spring-pot model which is the KVFD model with a negligible spring constant E_0.

2.2. Rheological models

In the next three sections, we provide equations describing both time and frequency domain behaviors of the three well established rheological models employed in this study, which clarifies the evaluation of their performances in later sections. The building blocks of these rheological models are shown in **Fig. 2**.

2.2.1. Kelvin-Voigt model

The Kelvin-Voigt (KV) model is one of the simplest models used to describe viscoelasticity in a material as a 2-parameter model consisting of a spring with Young's modulus E_1 and a dashpot element with viscosity η connected in parallel as depicted in **Fig. 2 (a)**. The KV constitutive equation describing the stress-strain relationship of a material in the time domain is:

$$\sigma(t) = E_1\varepsilon(t) + \eta\frac{d\varepsilon(t)}{dt} \tag{6}$$

From the constitutive equation, the stress relaxation response $\sigma_{SR}(t)$ to a ramp-and-hold strain application (Eq. (5)) is:

$$\sigma_{SR}(t) = \begin{cases} E_1\left(\frac{\varepsilon_0}{T_0}\right)t + \eta\left(\frac{\varepsilon_0}{T_0}\right) & t < T_0 \\ E_1\varepsilon_0 & t \geq T_0 \end{cases} \tag{7}$$

The behavior of a viscoelastic medium in the frequency domain under the KV model is obtained by taking the Fourier transform of the constitutive model (Eq. (8)) which gives the complex Young's modulus (Eq. (9)).

$$\hat{\sigma}(\omega) = E_1\hat{\varepsilon}(\omega) + \eta(j\omega)\hat{\varepsilon}(\omega) \tag{8}$$

$$\hat{E}(\omega) = \frac{\hat{\sigma}(\omega)}{\hat{\varepsilon}(\omega)} = E_1 + \eta(j\omega) \tag{9}$$

The SWS predicted by the KV model $c_{s,KV}(\omega)$ is then obtained by substituting Eq. (9) into Eq. (4):

$$c_{s,KV}(\omega) = \sqrt{\frac{2}{3\rho}\frac{E_1^2+\eta^2\omega^2}{\sqrt{E_1^2+\eta^2\omega^2}+E_1}} \tag{10}$$

In the *ideal* stress relaxation test under the KV model, the application of an ideal step strain requires an infinitely large force at the instance when strain (displacement) is applied, which is not realistic. When the *ideal* step strain is substituted by a more realistic ramp-and-hold strain, the KV model response as described by Eq. (7) shows some drawbacks. First, after the ramp period $t > T_0$, the model predicts that the material holds a constant stress level over time. However, this rules out one major characteristic of a viscoelastic material, which is the time-dependent decrease (relaxation) of stress under constant strain. Second, the stress at $t = 0$ is not zero, $\sigma(t=0) = \eta(\frac{\varepsilon_0}{T_0})$, based on the KV stress derivation as shown in Eq. (7), and $\sigma(t=T)$ is discontinuous.

2.2.2. Zener (standard linear solid) model

The Zener, or standard linear solid (SLS) model is a 3-parameter model with two spring elements (with Young's moduli E_1 and E_2) and one dashpot (η), as shown in **Fig. 2 (b)**. The constitutive equation of the SLS model is:

$$\sigma(t) + \frac{\eta}{E_2}\frac{d\sigma(t)}{dt} = E_1\varepsilon(t) + \frac{\eta(E_1+E_2)}{E_2}\frac{d\varepsilon(t)}{dt} \tag{11}$$

Similar to the derivations obtained from constitutive equation for the KV model in Section 2.2.1, the stress relaxation response to a ramp-and-hold strain application $\sigma_{SR}(t)$, the complex Young's modulus $\hat{E}(\omega)$, and the SWS for the SLS model $c_{s,SLS}(\omega)$ are described by Eqs. (12), (13) and (14), respectively. In Eq. (12), $U_{HeaviSide}(t)$ is the unit step function.

$$\sigma_{SR}(t) = \frac{\varepsilon_0}{T_0}\left\{\left(1-e^{-\frac{E_2 t}{\eta}}\right)\eta + E_1 t + \left(\left(e^{-\frac{E_2(t-T_0)}{\eta}}\right)\eta - (\eta + E_1(t-T_0))\right)U_{HeaviSide}(t-T_0)\right\} \tag{12}$$

$$\hat{E}(\omega) = \frac{\hat{\sigma}(\omega)}{\hat{\varepsilon}(\omega)} = \frac{E_1 + \frac{\eta(E_1+E_2)}{E_2}(j\omega)}{1+\frac{\eta}{E_2}(j\omega)} \tag{13}$$

$$c_{s,SLS}(\omega) = \sqrt{\frac{2}{3\rho}\frac{\left(\eta\omega E_2^2\right)^2 + \left(E_1E_2^2+\eta^2\omega^2(E_1+E_2)\right)^2}{\left(E_2^2+\eta^2\omega^2\right)\left(E_1E_2^2+\eta^2\omega^2(E_1+E_2)+\sqrt{\left(\eta\omega E_2^2\right)^2+\left(E_1E_2^2+\eta^2\omega^2(E_1+E_2)\right)^2}\right)}} \tag{14}$$

2.2.3. Kelvin-Voigt fractional derivative model

The Kelvin-Voigt fractional derivative (KVFD) model is a 3-parameter model comprised of a spring with Young's modulus E_0 and a spring-pot (fractional dashpot) characterized by two parameters of ξ and a as shown in **Fig. 2 (c)**. This model has been developed and applied to a range of soft tissue behaviors [29–35].

The parameter a quantifies the fractional order of the spring-pot element: when $a = 0$, the spring-pot acts as a spring and for $a = 1$ it behaves as a dashpot element. The second parameter ξ is the dashpot viscosity with the unit of $\text{Pa}\cdot\text{s}^a$. The constitutive equation for the KVFD model is described by Eq. (15) in which D^a denotes the fractional derivation.

$$\sigma(t) = E_0\varepsilon(t) + \xi D^a[\varepsilon(t)] \tag{15}$$

It is noted that when $a = 1$, the KVFD model reduces to a KV model, as Eqs. (6) and (9). Similar to the KV and SLS models, the KVFD stress relaxation response $\sigma_{SR}(t)$ to a ramp-and-hold strain is obtained from Eq. (16) and the complex Young's modulus as a function of frequency is:

$$\sigma_{SR}(t) = \frac{E_0\varepsilon_0}{T_0}(tU_{HeaviSide}(t) - (t-T_0)U_{HeaviSide}(t-T_0)) + \xi\frac{\varepsilon_0}{\Gamma(2-a)T_0}\left(U_{HeaviSide}(t)t^{1-a} - U_{HeaviSide}(t-T_0)(t-T_0)^{1-a}\right) \tag{16}$$

$$\hat{E}(\omega) = \frac{\hat{\sigma}(\omega)}{\hat{\varepsilon}(\omega)} = E_0 + \xi(j\omega)^a \tag{17}$$

where in Eq. (16) Γ refers to the gamma function. When E_0 is very small and thus negligible as shown by [12,36], for soft viscoelastic media, the KVFD model reduces to a 2-parameter model (the spring-pot model shown in **Fig. 2 (d)**) for which the SWS as a function of frequency is modeled by:

$$c_{s,KVFD}(\omega) = \sqrt{\frac{2}{3\rho}\frac{\xi}{\left[1+\cos\left(\frac{a\pi}{2}\right)\right]}}\omega^{\frac{a}{2}} \tag{18}$$

In Eq. (18), SWS is shown to follow a 2-parameter power-law relationship with the frequency under the KVFD model which is simplified as Eq. (19) considering that $\omega = 2\pi f$.

$$c_{s,KVFD}(f) = C_0 f^{\frac{a}{2}} \tag{19}$$

where C_0 is a reference speed at 1 Hz. The time domain and frequency domain relationships of these models are summarized in **Table 1**.

3. Methods

3.1. Sample preparation

Ex vivo bovine liver tissues were used in this work to study the time and frequency domain behavior of soft tissue. Whole fresh bovine liver was acquired from a slaughterhouse right after the animal was sacrificed and the liver was surrounded entirely by ice during delivery to our laboratory. The whole *ex vivo* bovine liver weighed approximately 6 kg. The liver was immediately immersed in normal isotonic saline solution (with 0.9% of sodium chloride dissolved in degassed water) to prevent tissue degeneration and dehydration and placed in a refrigerator overnight at 4°C. Using 0.9%-isotonic saline solution is a very common method for preserving the tissue samples over relatively short periods of time (< 24 h) in different studies involving tissue samples including some pathological experiments [37]. Therefore, it is considered a valid method for minimizing degradation in tissue samples in this study. On the following day, different samples were cut from the bovine liver for each of the four tests and allowed to reach room temperature (~20° C) while immersed in saline solution. Since small specimens dehydrate quickly and stiffen when exposed to air, each sample was kept immersed in normal saline solution until just prior to testing to avoid any possible dehydration of the samples, which could affect the measurements of stress and SWS. The whole bovine liver used in this study is shown in **Fig. 3 (a)**.

Table 1
Comparison of time domain and frequency domain relationships of the rheological models.

	Model	Time domain behavior	Frequency domain behavior
2-parameter	KV	$\sigma(t) = E\varepsilon(t) + \eta\frac{d\varepsilon(t)}{dt}$	$\hat{E}(\omega) = E_1 + \eta(j\omega)$
3-parameter	SLS	$\sigma(t) + \frac{\eta}{E_2}\frac{d\sigma(t)}{dt} = E_1\varepsilon(t) + \frac{\eta(E_1+E_2)}{E_2}\frac{d\varepsilon(t)}{dt}$	$\hat{E}(\omega) = \frac{E_1 + \frac{\eta(E_1+E_2)}{E_2}(j\omega)}{1+\frac{\eta}{E_2}(j\omega)}$
3-parameter	KVFD	$\sigma(t) = E_0\varepsilon(t) + \xi D^a[\varepsilon(t)]$	$\hat{E}(\omega) = E_0 + \xi(j\omega)^a$
2-parameter	Spring-pot	$\sigma(t) = \xi D^a[\varepsilon(t)]$	$\hat{E}(\omega) = \xi(j\omega)^a$

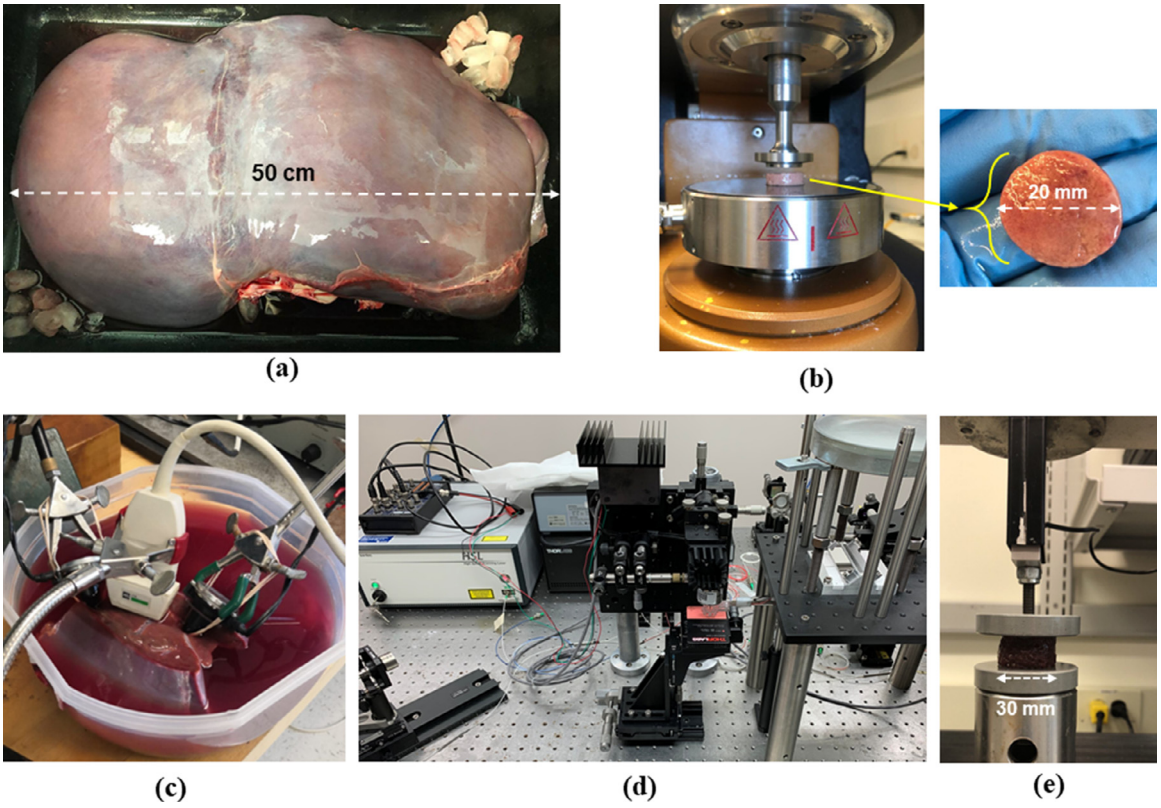

Fig. 3. (**a**) Whole fresh bovine liver, (**b**) experimental test setup of the rheometer for harmonic rotational shear test with a cylindrical liver sample, (**c**) ultrasound experimental setup using the Verasonics ultrasound system and transducer in place with two miniature vibrator sources located at different positions and in contact with the liver sample tissue as RSW sources, (**d**) OCE setup using a custom-built phase sensitive swept-source optical coherence tomography system (**e**) experimental setup for stress relaxation test with a liver sample in place.

3.2. Experimental studies

Four independent tests were employed to provide a comprehensive range to assess the rheological models' performance in the frequency and time domains. To investigate the dispersion behavior of liver tissue samples at discrete frequencies from 1 Hz to 1 kHz, three independent experimental tests were performed: (i) harmonic shear test, (ii) reverberant shear wave (RSW) ultrasound (US) scans, and (iii) optical coherence elastography (OCE) scans based on RSW. The test set-ups for these three experiments are shown in Fig. 3 **(b), (c)** and **(d)**. The harmonic shear test was employed in assessing the speed dispersion behavior at low frequency ranges, i.e., 1 Hz to 15 Hz. The RSW-US approach provided the speed dispersion at mid-range frequencies of 200 Hz to 400 Hz. The RSW-OCE approach was used to quantify the speed dispersion behavior at 1 kHz, which is outside the scope of the RSW-US test due to high noise and attenuation, and outside the scope of the rheometer test due to the low-frequency limitations of that approach. To study the time domain behavior of *ex vivo* bovine liver tissues, stress relaxation test was done on small liver samples; its experimental setup is shown in Fig. 3 **(e)**. All four tests were done on the same day while the samples were at approximately 20°C and at similar hydration conditions in order to make the results from all four approaches as consistent as possible. The room temperature was maintained during all testing periods using a wall-mounted digital thermostat, and the temperature of the samples was frequently measured using a digital infrared laser thermometer (Model LASERGRIP 1080, Etekcity brand, Vesync Inc., Anaheim, CA, USA) while the samples were resting in saline solution until they reached room temperature. Each of the three tests in the frequency domain were tailored to target their optimal frequency range. A minimum of three liver samples, free of ligaments and major arteries, were used for each test. In the case of RSW-US, scan planes of 4 cm × 5.5 cm were analyzed for shear wave speed. The detail for each measurement is presented in the following four sections.

3.2.1. Harmonic frequency sweep shear test

The frequency sweep rotational shear test enables the characterization of the viscoelastic bovine liver within a range of frequencies. For performing this test, a hybrid rheometer (Discovery Series HR-2, TA Instrument Inc., New Castle, Delaware, USA) was

employed with a 20 mm diameter flat platen geometry. The diameter of liver sample cuts for the test were also 20 mm. To determine the linear viscoelastic region (LVER) over the strain amplitude in the shear test, first the amplitude sweep test was done on the liver tissue at the frequency of 5 Hz, which is explained in detail in the Appendix A. Based on that, the strain amplitude of 0.7% was chosen within the LVER as the amplitude for performing the frequency sweep test, in which the storage and loss shear moduli were the experimental outputs for the frequency range of 1 Hz to 15 Hz. The SWS as a function of frequency is then obtained from the measured shear moduli using Eq. (4) which is model-independent (Young's modulus and shear modulus are related by Eq. (2)).

3.2.2. RSW ultrasound approach

RSW vibration sources. Two small identical vibration sources (Model DAEX320-8, 8 Ohm, 20 W, Dayton Audio, Ohio, USA) were put in contact with the *ex vivo* liver tissue as shown in **Fig. 3 (c)**; these generated the RSW within the tissue for the ultrasound scan. To create an effective contact surface between each vibration source and the tissue, a conical knob was attached and fixed on each source as shown in the figure. These vibrator sources were connected to a power amplifier (BKA1000-4A, ButtKicker, Westerville, OH, USA) driven by a dual-channel function generator (AFG3022B, Tektronix, Beaverton, OR, USA) which provided input signals to the vibration sources. Vibration frequency ranges between 200 – 400 Hz were used for the *ex vivo* liver experiment.

Ultrasound scanner and data acquisition. A Verasonics ultrasound scanner (V-1, Verasonics, Kirkland, WA, USA) connected to a linear ultrasound probe (model L7-4, ATL, Bothell, WA, USA) was used to track the induced displacements using a Loupas estimator [38]. The center frequency and the sampling frequency were 5.21 MHz and 20 MHz, respectively. The frame rate was set to 5000 Hz and the total acquisition time was 0.25 s.

The SWS was measured by examining the phase distribution of the reverberant field. Recently, Ormachea and Parker [39] demonstrated that the reverberant phase gradient was proportional to the local wavenumber. This phase estimator is less sensitive to imperfections in the reverberant field distribution and requires a smaller support window compared to earlier estimators based on autocorrelation. The specific details of the phase velocity estimator are described in [39].

3.2.3. Optical coherence elastography (OCE)

OCE scanner set-up and excitation sources. A swept-source optical coherence tomography (SS-OCT) system was used in conjunction with a mechanical excitation system to form the entire custom-built OCE system. The SS-OCT system was implemented with a swept-source laser (HSL-2100-HW, Santec, Aichi, Japan) with a center wavelength of 1310 nm and a bandwidth of 140 nm. The lateral resolution was approximately 20 μm and the axial resolution was approximately 6 μm in air. The SS-OCT system and the mechanical excitation system were both controlled using LabVIEW software (Version 14, National Instruments, Austin, Texas, USA). The sample dimensions for the OCE scans were approximately 3 cm $\times$ 3 cm $\times$ 4 cm.

The mechanical excitation system consists of the following: a function generator (AFG320, Tektronix, Beaverton, Oregon, USA) that provides the 1 kHz continuous sinusoidal excitation signal, an amplifier (PDu150, PiezoDrive, Callaghan, NSW, Australia), a piezoelectric actuator (BA4510, PiezoDrive, Callaghan, NSW, Australia), and a custom circular ring with 8 points of contact to induce reverberant shear waves. The field of view was a 5 $\times$ 5 mm area used to scan a homogeneous region of liver tissue.

OCE data acquisition and processing. The MB-mode acquisition approach was used to acquire 3D reverberant OCE data [40]. One hundred (100) A-lines by 100 frames by 100 M-mode measurements were acquired. The estimated particle motions were obtained using the algorithm developed by Loupas et al. [38].

Two-dimensional (2D) spatial autocorrelations for each *xy*-plane were calculated with a square window area of 1 mm^2. The local wavenumber k was then estimated via curve fitting and, subsequently, SWS could be calculated. This process was repeated at each depth to construct the 3D SWS maps. The average SWS and standard deviation (STD) in the cropped 3D region of interest (ROI) were reported. All data processing was performed using MATLAB 2020b (Mathworks, Inc., Natick, MA, USA).

3.2.4. Stress relaxation test approach

The SR test was implemented using a Q-Test/5 machine (MTS, Eden Prairie, MN, USA) similar to previous studies [28,36]. The test was performed using a 5 N load cell with a compression rate of 0.5 mm/s. The strain applied was 10% strain ($\frac{\text{mm}}{\text{mm}} \times 100$) which was exerted linearly from zero to a maximum of 10% over a short time ($\sim$ 3.5 s) and then the strain was kept constant during the relaxation period for approximately 350 s. The output from the SR test was the variation of force recorded by the load cell over time for each sample during the whole test period.

The measured force is then converted to stress $\sigma(t)$ by incorporating the cross-sectional area of each sample and then the SR curves are fitted to each rheological model to assess how well each model captures the time domain behavior of the liver tissue.

The curve fitting was done using MATLAB 2020b (Mathworks, Inc., Natick, MA, USA) using the least square method based on minimization of errors between test data and the fitted curve, including the final fit of all frequency domain data to the different rheological models.

4. Results

4.1. Preloading effect

The viscoelastic properties of liver tissues measured in an experiment may change due to factors associated with the test conditions. An important factor is the preloading effect due to the tissue weight in tall vertical cylindrical samples. Preloading is known to result in an increase in the shear modulus and therefore, measured stiffness level [41, 42]. As observed in **Fig. 4,** the liver sample bears a length reduction of over 20% due to its own weight in position **(b)** compared to **(a)**. According to the study by Tan et al. [43], a strain of 20% results in stiffening of the modulus in bovine liver by a factor of 3/2, or a 50% increase. In this study, 20% preloading is assumed in the stress relaxation, RSW-US, and OCE tests, which is compensated by the factor 2/3 for the shear modulus as a first-order correction for the pre-strain. It is noted that the rheometer test is not adjusted as the samples employed for performing the harmonic shear test had a comparatively smaller ratio of height to diameter and also minimal contact force by the test plate.

4.2. Rheometer shear test results

Fig. 5 shows the results obtained from the harmonic shear test using the rheometer on three bovine samples where **(a)** shows the storage and loss shear moduli for the samples measured by the rheometer, and **(b)** indicates the SWS calculated from the moduli in **(a)** at low frequency range, (1 Hz $\leq f \leq$ 15 Hz).

4.3. RSW ultrasound approach

Fig. 6 presents the results of the RSW-US approach for a sample frequency of 360 Hz. In this figure, **(a)** shows the gray scale

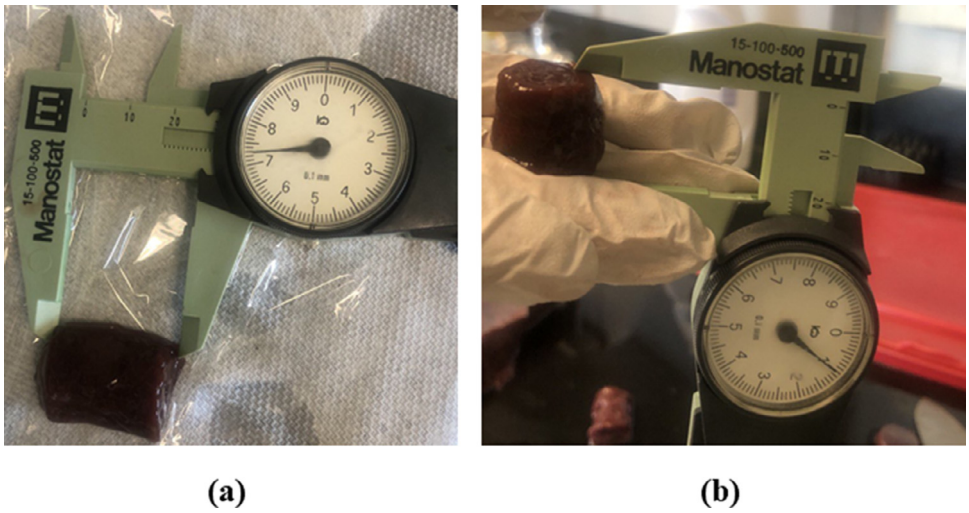

Fig. 4. Difference in height measurement of a liver sample for stress relaxation experiments in two different positions in (a) and (b). The vertical positioning of a tall cylinder for testing results in an over 20% reduction of height due to gravity acting on the compressible mass.

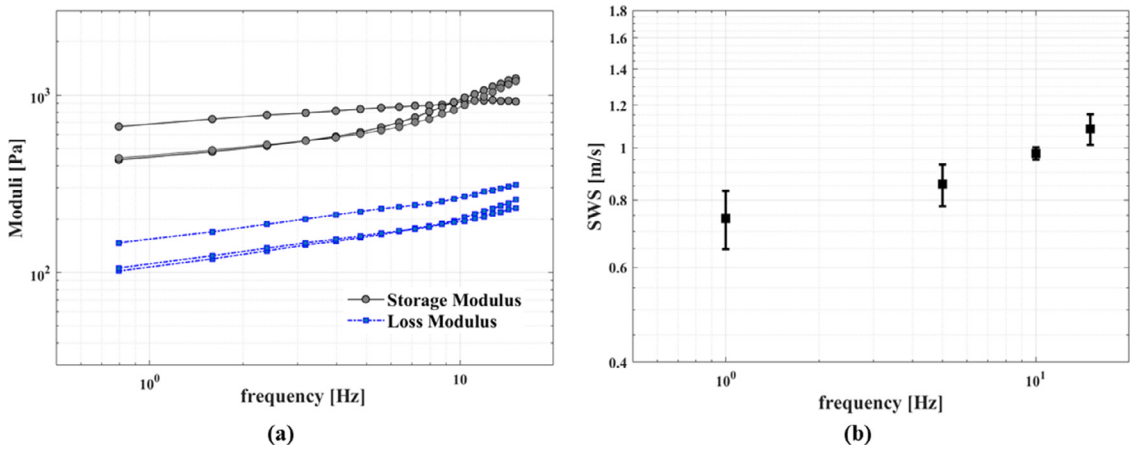

Fig. 5. Rheometer shear test results on three liver samples: (a) storage (black curves) and loss (blue curves) shear moduli, (b) SWS obtained at the low frequency range using Eq. (4).

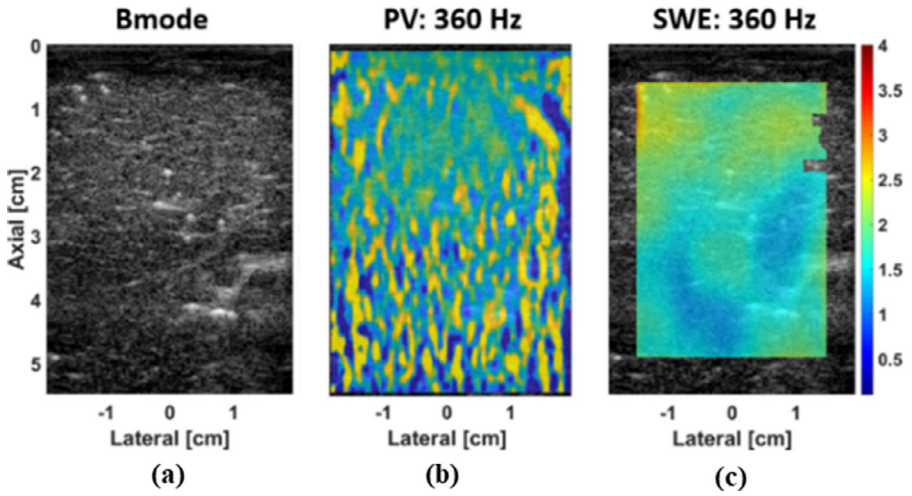

Fig. 6. **(a)** B-mode image of the liver, **(b)** particle velocity illustrating the shear wave propagation and the RSW field produced within the ROI, **(c)** final elastographic image using the phase gradient method in a reverberant field.

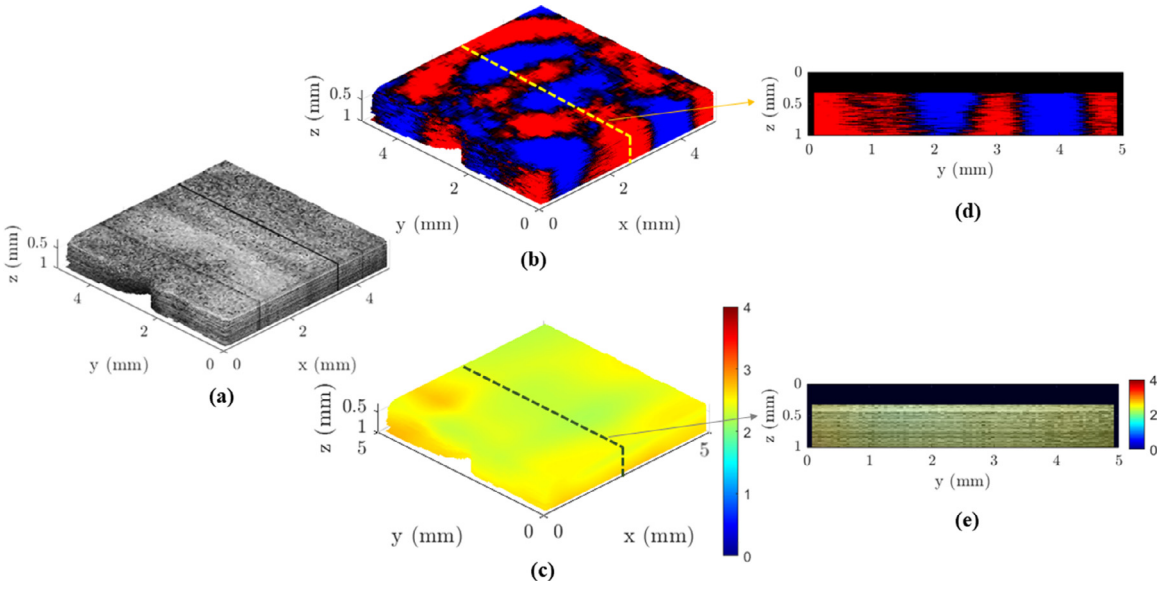

Fig. 7. (a) 3D B-mode image (0 to 255 grayscale) of homogeneous liver ROI. (b) Sample 3D frame showing reverberant shear wave pattern. (c) Estimated 3D shear wave speed map (d) 2D RSW field within the plane cut though middle of 3D RSW, (e) 2D SWS on a plane cut though middle of part (c).

B-scan of the liver under experiment, **(b)** is the RSW field shown as the particle velocity produced within the domain by external mechanical excitation, and **(c)** depicts the elastography images for local SWS overlaid on the B-scan image.

4.4. RSW optical coherence elastography approach

The RSW-OCE results for SWS measurement at the frequency of 1 kHz is shown in Fig. 7 in which **(a)** is the 3D gray-scale B-scan ROI of a bovine liver sample, **(b)** shows a sample frame in time of the 3D RSW generated within the sample, and **(c)** is the estimated SWS within the 3D sample obtained from the analysis of OCE data. It is noted that the RSW-OCE approach provides characterization of SWS within a 3D domain, not only along a 2D surface, but also along the axial (depth) direction. It is not solely based on surface wave propagation; it incorporates the propagation of random shear waves diffusing in different directions within the volume. To see how the RSW field and SWS appear inside the domain, a 2D plane cut through the middle of the 3D domain along the *x* axis was selected and the RSW and SWS are shown within this 2D plane in Fig. 7 **(d)** and **(e)**, respectively. It is noted that Fig. 7 **(d)** demonstrates how uniform the local SWS is within the 3D domain of the small liver sample tested. The test is repeated for three different liver samples. The average value and the standard deviation of the 3D estimated SWS are reported.

To summarize the frequency domain SWS measurements for *ex vivo* bovine liver tissue from the three experiments, Fig. 8 **(a)** visualizes the results from the rheometer shear test, the RSW-US scan, and the RSW-OCE experiment with the standard deviation for SWS measurements at each frequency shown as errorbars. These cover the range of 1 Hz -1 kHz shear wave frequencies. There are gaps between the three measurement techniques, however all rheological models considered would predict smooth transitions between the respective measurement bands.

4.5. Stress relaxation test results

Fig. 8 **(b)** shows the experimental SR curves obtained from mechanical tests over a relaxation time span of 350 s, representing the time domain behavior of *ex vivo* bovine liver tissues.

5. Discussion

Having obtained SWS measurements over a wide frequency range and the time domain SR measurements using independent experimental approaches, the key question before us is: *which rheological model will best predict the behavior in soft liver tissue, in both frequency and time domains, consistently and with the fewest parameters?*

5.1. Performance of rheological models

In addressing the question raised above, we employed the two different approaches (approach A and approach B) shown in Fig. 1 to investigate the performance of the rheological models in predicting the *ex vivo* bovine liver tissue behavior in both frequency and time domains.

5.1.1. Approach A: Frequency domain data analysis

For the first approach in evaluating the performance of three rheological models, we fit the frequency domain SWS data obtained from our three experiments to dispersion relationships of the three models. The analyses are presented in Fig. 9 **(a), (b),** and **(c)** for the KV, SLS and KVFD models, respectively, in log-log scale with the SWS dispersion fitting parameters reported in Table 2.

As observed in these figures, all three models are capable of capturing the SWS dispersion within the middle range of frequencies, similar to observations in other studies [44]. However, the models differ in how they behave at lower frequencies, i.e., $f \leq$ 10 Hz and high frequencies ($f = 1$ kHz). The KV model in Fig. 9 **(a)** exhibits a constant SWS (negligible dispersion behavior) at the lower frequency end. However, the experimental SWS measurements obtained from the rheometer test as well as the SWS dispersion reported for human brain by Herthum et al. [15] show highly dispersive behavior of soft tissues in this frequency range. It is also noted that the KV model, based on observations by Nightingale et al. [7], shows large variations of its fitting parameters over limited frequency ranges, therefore, it is not well suited for characterizing highly dispersive media such as human liver. These are important limitations in employing the KV model for the frequency domain analysis.

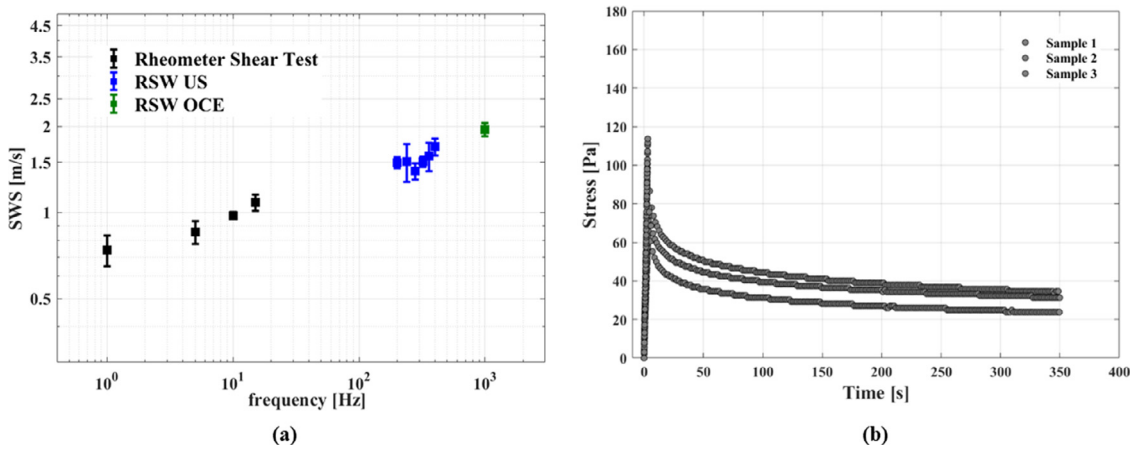

Fig. 8. (a) Frequency domain SWS data obtained from the three different experimental techniques. (b) Time domain SR test results for three *ex vivo* bovine liver samples.

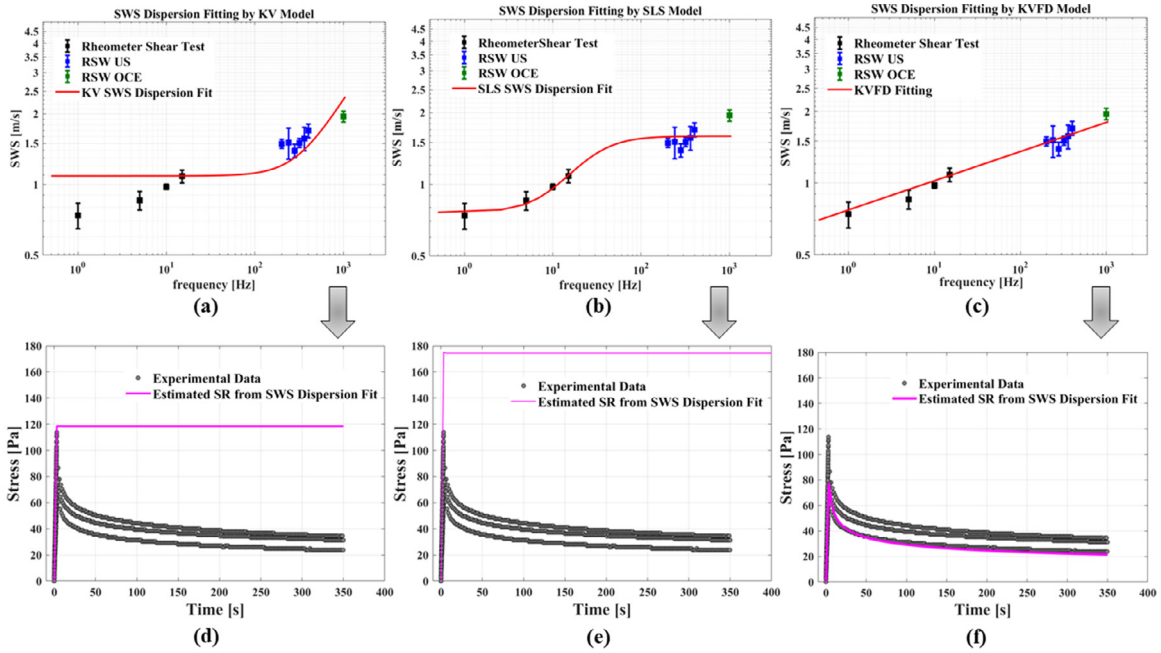

Fig. 9. Results from Approach A. Top Row: SWS data from three independent tests on bovine liver samples fitted to the: (a) KV model, (b) SLS model, and (c) KVFD model. Bottom Row: stress relaxation curves *predicted* from SWS dispersion fitting results shown as purple curves for (d) KV model, (e) SLS model, and (f) KVFD model, compared with the actual experimental stress relaxation measurements.

Table 2
Fitting parameters obtained fitting the experimental SWS data of liver samples to KV, SLS, and KVFD models in Fig. 9 (a), (b), and (c), respectively.

	SWS dispersion fitting parameters			Goodness of fit
KV model	$E_1 = 1184$ Pa	$\eta = 0.532$ Pa.s		$R^2 = 0.60$
SLS Model	$E_1 = 1744$ Pa	$E_2 = 5886$ Pa	$\eta = 24.03$ Pa.s	$R^2 = 0.86$
KVFD Model	$E_0 = 5.46 \times 10^{-6}$ Pa	$a = 0.245$	$\xi = 1097$ Pa.s^a	$R^2 = 0.96$

The SLS model in **Fig. 9 (b)** performs well in describing the SWS dispersion behavior at low frequencies as also observed by Klatt et al. [45], however for the higher range of frequencies provides less accurate results. The SLS model incorporates one additional parameter in comparison to the KV model, however the SLS fitting accuracy is still not accurate enough for SWS dispersion modeling.

The KVFD model in **Fig. 9 (c)** provides an excellent fit to the experimental SWS dispersion data with a value of E_0 being negligible, resulting in a 2-parameter SWS dispersion model with accurate results. It performs well both in terms of goodness of fit over the wide range of frequencies as well as employing the fewest number of significant fitting parameters.

Let us go one step further in evaluating the performance of the three rheological models using approach A to see how the parameters from frequency domain analysis project onto the time domain behavior. To do so, we employed the fitting parameters obtained from the analysis of SWS in **Table 2** to *predict* the corresponding time domain SR and then compared it with the actual experimental measurements of SR for bovine liver to see how prediction is close to the real behavior. The resulting *estimated* SR curves are

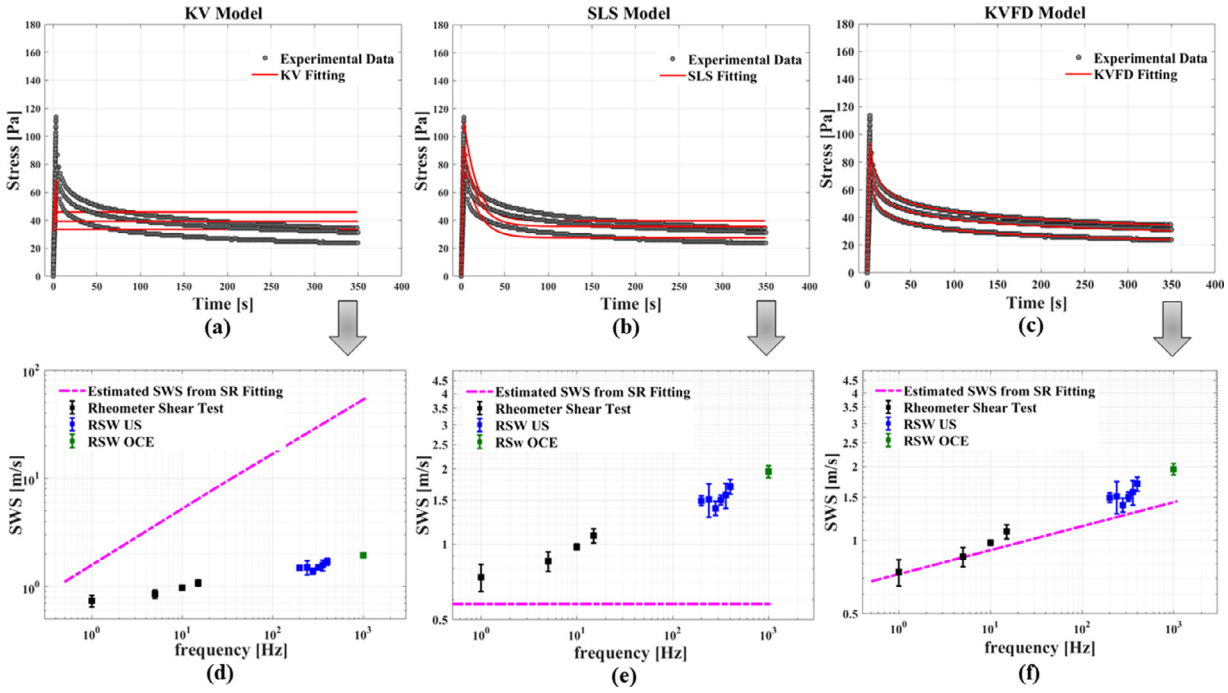

Fig. 10. Results from Approach B. **Top Row:** stress relaxation data from bovine liver testing fitted to the: **(a)** KV model, **(b)** SLS model, and **(c)** KVFD model. (The results on three different liver samples indicate the reproducibility of the test.) **Bottom Row:** SWS dispersion *predicted* from SR test fitting parameters shown as purple curves for **(d)** KV model (the range of vertical axis for SWS is extended to 100 m/s to show the unusually large range of *predicted* SWS by the KV model), **(e)** SLS model, and **(f)** KVFD model, compared with the actual experimental SWS measurements.

shown in Fig. 9 **(d), (e),** and **(f)** for the three rheological models as purple lines.

Fig. 9 **(d)** and **(e)** for the KV model and SLS model, respectively, estimate a SR behavior dramatically departing from the experimental data in terms of the shape by which stress relaxes over time as well as the stress level . The KV model indicates a constant SR behavior originating from the nature of its SR formula in Eq. (7). On the other hand, the stress in the SLS model is dominated by the strong constant term such that its exponential decay term is relatively small, producing what appears to be an almost constant stress. The orders of magnitudes of the SLS parameters (E_1, E_2, and η) obtained from SWS dispersion fitting causes this SR response. To elucidate this stress behavior of the SLS model, we obtain its single time constant from SLS fitting results in Table 2 which is equal to $\tau = \frac{\eta}{E_2} = \frac{24.03}{5886} = 0.004$ s. This characteristic time constant is very small, corresponding to a fast decay time incorporated within the model, resulting in failure of the SLS model in estimating the appropriate SR behavior. For the KVFD model in Fig. 9 **(f)**, the SR curve *predicted* from the SWS dispersion fitting parameters shows a reasonable SR response in terms of both the shape of the SR behavior and the magnitude of stress in comparison to the experimental SR data.

5.1.2 . Approach B: Time domain data analysis

For the second approach, we start from analysis of time domain experimental data measured in the SR test. Fig. 10 (top row) shows the experimental SR data of the *ex vivo* bovine liver tissues for three different samples fitted to SR relationships of the three rheological models: **(a)** KV model, **(b)** SLS model, and **(c)** KVFD model presented as red solid lines. All curve fitting was performed for the entire ramp-and-hold strain period. The average fitting parameters over three samples are reported in Table 3 for each model.

Looking at the KV model fitting results in Fig. 10 **(a)**, the model captures the stress behavior of the experimental data during the ramp strain application period ($0 < t < T_0$), but it fails to correctly predict the SR behavior when constant strain is applied ($t > T_0$). Specifically, this model prescribes a constant stress value for the relaxation period ($t > T_0$), which is unrealistic. The SLS model in Fig. 10 **(b)** demonstrates an improvement over the KV model in terms of describing the SR behavior of the liver tissues, as it shows a decaying (rather than constant) stress for $t > T_0$. However, the SLS model is not able to capture the experimental relaxation behavior of liver with any reasonable accuracy. The KVFD model in Fig. 10 **(c)** predicts the viscoelastic relaxation behavior of *ex vivo* bovine liver tissue very well for the entire ramp-and-hold strain application period. The KVFD model incorporates a spectrum of the relaxation time constants, which results in capturing a range of time constants and therefore, provides more flexible and accurate fitting results than the SLS model with a single time constant. Also, it is notable that for the KVFD model SR fitting, the parameter E_0 takes a negligible value which permits the reduction to a 2-parameter model with accurate results.

In the Appendix B, the results from fitting the experimental SR data to the three rheological models for shorter relaxation period ($0 < t < 100$ s) than Fig. 10 are presented. This analysis shows similar performances for the three models where the KV and SLS models fail to reasonably fit the time domain behavior while the KVFD model shows an excellent agreement with the SR data.

To assess how the results obtained from time domain analysis of experimental SR data would project onto the behavior in the frequency domain under each rheological model, the fitting parameters from SR fittings in Fig. 10 **(a)–(c)** and Table 3 are employed to estimate the corresponding SWS. Then, these SWS *predictions* from all models are compared with the actual experimental measurements of SWS for bovine liver to see how close the predictions are to the actual measurements. The results are demonstrated in Fig. 10 **(d), (e),** and **(f)** for the KV model, SLS model, and KVFD model, respectively.

Looking at the predicted SWS dispersion for the KV model in Fig. 10 **(d)**, we observe an elevated order of magnitude of SWS values in the plot compared to experimental SWS measurements. The range of SWS for soft tissues such as liver is 0.7 m/s to 2.0

Table 3
Fitting parameters obtained from fitting the experimental SR data of liver samples to KV, SLS, and KVFD models in Fig. 10 (a), (b) and (c), respectively. Results are averaged over three samples' measurements with the STD reported in parentheses.

	SR averaged fitting parameters (STD)			Goodness of fit
KV model	$E_1 = 395.2$ Pa (62.1)	$\eta = 676.2$ Pa.s (365.5)		$R^2 = 0.47$
SLS Model	$E_1 = 342.9$ Pa (61.7)	$E_2 = 657.1$ Pa (116.0)	$\eta = 10239$ Pa.s (1369.5)	$R^2 = 0.93$
KVFD Model	$E_0 = 3.33 \times 10^{-5}$Pa (2.0×10^{-7})	$a = 0.20$ (0.008)	$\xi = 1075$ Pa.s^a (163.7)	$R^2 = 0.98$

m/s over a wide frequency span, observed in this study as well as other literature for human brain [15] and human liver [39]. Therefore, the time domain fitting parameters for KV models does not represent a realistic frequency domain behavior.

For the SLS model in **Fig. 10 (e)**, the estimated SWS response in the frequency domain is not only far off compared with the actual SWS measurements, but the SWS estimation produces a negligible SWS dispersion (frequency-dependent) behavior. This is in conflict with the fundamental dispersive behavior of viscoelastic soft tissues such as liver. Therefore, modeling the time domain SR data using the SLS model does not map to an accurate frequency domain behavior. Going further in evaluation of the SLS model's performance, its single time constant from SR fitting parameters in **Table 3** is $\tau = \frac{\eta}{E_2} = 15.6$ s. The time domain gives one relatively large (and therefore slow) time constant τ which in the frequency domain corresponds to a low frequency.

Fig. 10 (f) shows the SWS for bovine liver tissue estimated by the KVFD model using the parameters from the SR time domain behavior. The results appear reasonable in terms of the range of SWS approximated for the liver tissues (0.7 m/s to 2.0 m/s) as well as the prediction of a non-zero SWS dispersion behavior. Therefore, for the KVFD model, the time domain behavior predicts the frequency domain behavior reasonably well.

It is noted that the general trend observed in the behavior of *ex vivo* bovine liver SWS measurements such as dispersive behavior and the range of variation are consistent with other *in vivo* measurements of human liver [8] and human brain [15]. Therefore, KV and SLS models are expected to show similar limitations in describing the *in vivo* measurements for these soft tissues. Also, the KVFD model has been applied to other soft tissues such as prostate [12] and lung tissue [46] and therefore, the results of this study may be applicable to other tissues, as well.

5.2. Which model is the most appropriate?

The investigations into the performance of KV, SLS, and KVFD rheological models from both the time domain and frequency domain perspectives showed that the KVFD model performs well in both direct fitting to experimental SR data in the time domain and also direct fitting to experimental SWS dispersion data in the frequency domain. Moreover, this model was successful in consistently predicting (modeling) the material behavior in one domain (time or frequency) from independent measurements in the other domain. The KV and SLS models were shown to be incapable of describing elementary time domain (SR) behavior of liver tissues. Also, although their SWS dispersion behavior in the frequency domain can reasonably match the SWS experimental data within limited frequency ranges, those results do not map to a corresponding reasonable behavior in the time domain. Therefore, the KVFD model is demonstrated to be the only model to comprehensively describe liver tissues properties in both time and frequency domains. It is noted that the KVFD model reduces to a 2-parameter model in practice since the parameter E_0 usually takes a negligible value in both time and frequency domain analysis of viscoelastic tissues such as liver as shown in other studies [12,36], and reduces to a spring-pot model as shown in **Fig. 2 (d)**. It is worth highlighting that the 2-parameter KVFD model is a power-law model in line with the frequent occurrence of power-law phenomena in nature [47,48]. Thus, our study indicates that the KVFD model best describes the material's behavior with the fewest number of parameters.

Moreover, comparing the performances of the three rheological models from the Akaike information criterion (AIC) [27], which aims at selecting the best model based on the joint analysis of model's complexity (number of parameters) and model's ability to capture experimental measurements well, the KVFD model performs better than the KV and SLS models. The detailed results of these comparisons based on the AIC are presented in Appendix C.

It is worth noting that based on assessments of common rheological models in nonlinear regimes from computational simulations [49], the fractional derivative models are suggested to describe more diverse simulating conditions than the classical models. This is aligned with the conclusion made in this study based on the analysis of a range of experimental measurements of viscoelastic liver tissues in or near the linear, small strain regime. Furthermore, a recent comparative study of three nonlinear models of liver under strains up to 50% found that a model with an exponential strain energy term and a fractional derivative term was superior to others [50]. Interestingly, their fractional derivative exponent was found to be $a = 0.2$ to 0.25 depending on which error norm was used. This compares closely with our results in **Tables 2** and **3** where the KVFD exponent is $a = 0.2$ and 0.254 for the different tests.

We now turn to a potential point of objection concerning the spring-pot model for soft tissues. With its fractional derivative, it might seem abstract and not connected to simple physical mechanisms. However, the derivation of the spring-pot model from multiple parallel elements in a Maxwell model is actually simple and straightforward. This arrangement of multiple parallel elements and an optional single spring element is the generalized Maxwell-Weichert model [51] and has longstanding history as a useful multi-scale, multi-time constant model. Now let us assume the distribution of time constants in the generalized Maxwell model is a power-law distribution characterized by parameter b where $b > 1$. A strong rationale for introducing a power-law function is that the power-law distribution is frequently found to describe multi-scale systems in nature and biology [52,53]. Incorporating the power-law assumption within the generalized Maxwell model, shown in detail in the Appendix D, yields precisely the spring-pot model, with the associated time and frequency domain behavior similar to the form shown in **Table 1**. In particular, the stress relaxation will be of the power-law form proportional to $\frac{1}{t^{b-1}}$ for $b > 1$, and the complex modulus $\hat{E}(\omega)$ will be a power-law proportional to ω^{b-1} for $b > 1$ [26,54].

Thus, the concept of the spring-pot may seem abstract for modeling soft tissues, but it actually results simply from the realistic

acknowledgement that the components of soft tissues are multi-scale both in size and in time constants.

Limitations of this work include the need for higher frequency shear wave data (above 1 kHz) and the measurement of other soft vascularized tissues. Furthermore, there is a need to better understand how diseases and pathologies affect the viscoelastic properties. This study also has not explicitly considered nonlinear models of tissue behavior. These have shown promise in describing behaviors seen in situations with larger imposed strains [49,50,55–58]. Finally, the extension of these results to *in vivo* tissue with blood flow and pressure requires further study. *In vivo* measurements of shear wave phase velocity and dispersion are now possible [59], however direct comparison of *in vivo* to *ex vivo* or post-mortem studies are limited.

6. Conclusion

The KVFD model was shown to perform consistently well in fitting to stress relaxation experimental data in the time domain as well as fitting to SWS dispersion in the frequency domain for experimental data measured from four independent techniques. This model was also successful in predicting the material behavior in one domain (time or frequency) from independent measurements in the other domain. On the other hand, the KV and SLS models were shown to be grossly incapable of describing time domain behavior of liver tissues under simple stress relaxation conditions. This difference originates from the fact that the KVFD model includes a spectrum of relaxation time constants from small to large, which allows this model to capture the liver relaxation behavior well, while the SLS and KV models offer only one single relaxation time constant, which results in unreasonable fitting results. When examining SWS dispersion behavior in the frequency domain, the KV and SLS models could partially fit the SWS experimental measurements within a limited frequency range, however those results did not map to a corresponding reasonable behavior in the time domain. Moreover, it is noted that the KVFD model can be reduced to a 2-parameter model in practice in both domains (a spring-pot model). Therefore, the KVFD model is found to be the most accurate model to comprehensively describe the material properties in both the time and frequency domains while also more efficiently using the fewest number of parameters.

Declaration of Competing Interest

The authors declare no potential conflicts of interest with respect to this article.

Acknowledgments

This work was supported by National Institutes of Health Grants R21EB025290, R21AG070331, and F30AG069293.

Appendix A. Amplitude sweep test for linear viscoelastic region (LVER)

Before performing the oscillatory frequency sweep shear test to characterize bovine liver behavior at low frequencies, first it is crucial to find the suitable range of shear strain amplitude to assure not exceeding the LVER of the liver tissues. Within the LVER, the stress applied on the sample does not alter its internal structures and therefore, does not change its rheological properties, such as storage modulus.

To this end, the oscillatory strain amplitude sweep test was done on *ex vivo* bovine liver samples using a rheometer (Discovery Series HR-2, TA Instrument Inc., New Castle, Delaware, USA) to ensure selecting a suitable strain amplitude as a critical parameter for the subsequent frequency sweep test. The amplitude sweep test was performed at a constant frequency of 5 Hz for a strain amplitude range of 0.1% up to 6% and the storage and loss moduli were reported as a function of strain %. Fig. A.1 shows an example of the amplitude sweep test results on a bovine liver sample indicating the LVER. Experiments on different samples demonstrated that the strain level of 0.7% lies within the LVER and is a reasonable strain amplitude to apply in the frequency sweep test.

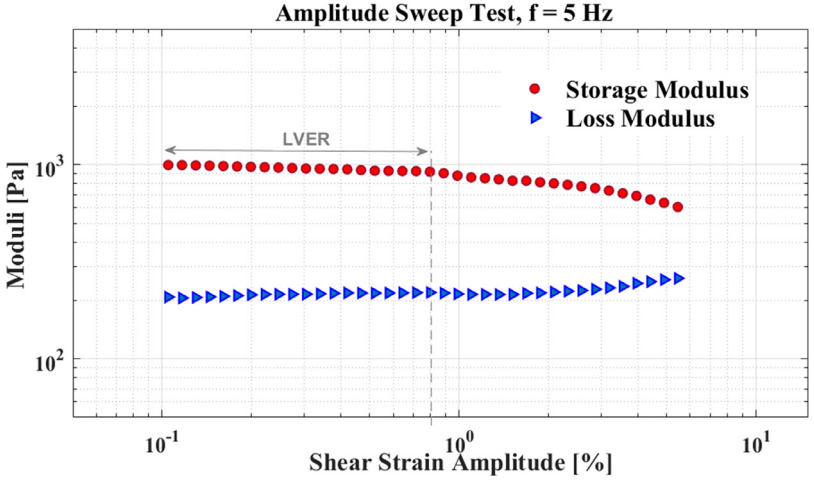

Fig. A.1. Harmonic strain amplitude sweep test results on a bovine liver sample.

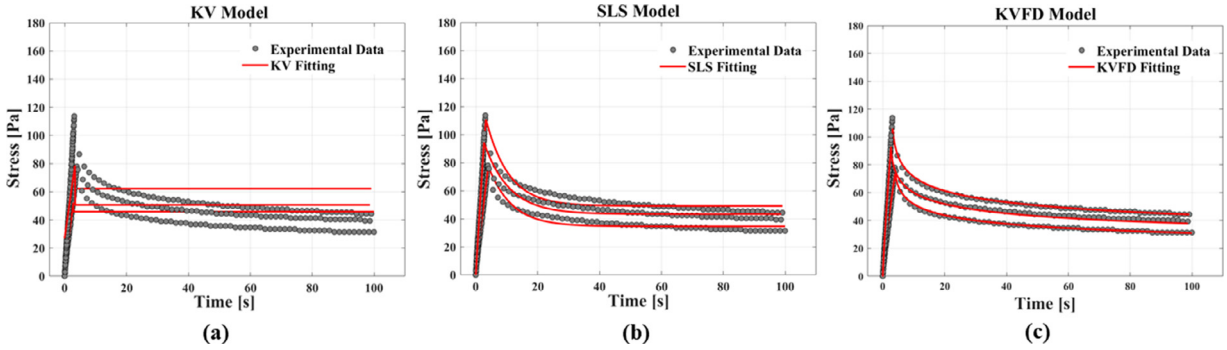

Fig. B.1. (a) KV, (b) SLS, and (c) KVFD models fit to the liver SR test data for only 100 s (short time interval).

Table B.1
Rheological models' fitting parameters obtained from fitting SR test data for 100 s (short time interval). Results are averaged over three samples' measurements with the STD reported.

	SR Averaged Fitting Parameters (STD)			Goodness of fit
KV model	$E_1 = 528.9$ Pa (83.6)	$\eta = 502.0$ Pa.s (380.7)		$R^2 = 0.56$
SLS Model	$E_1 = 423.5$ Pa (72.9)	$E_2 = 637.4$ Pa (112.1)	$\eta = 4869.5$ Pa.s (755.3)	$R^2 = 0.96$
KVFD Model	$E_0 = 5.77 \times 10^{-4}$ Pa (1.6×10^{-6})	$a = 0.195$ (0.006)	$\xi = 1050$ Pa.s^a (165)	$R^2 = 0.99$

Appendix B. Effect of relaxation period on SR fitting results

Fig. B.1 presents the results of SR fitting to three rheological models for shorter time periods (100 sec.) than Fig. 10 **(a), (b)** and **(c)**. Physically, this corresponds to eliminating slower (larger) characteristic time scales from the liver SR behavior. It is observed that the performance of the SLS model improved to some degree compared to Fig. 10 **(b)**, however it is still not a reasonable fit. The KVFD model works best in describing the material behavior due to the nature of the model including a spectrum of characteristic time constants. The fitting parameters are also consistent (varying slightly) with the values reported for longer fitting periods in Table B.1.

Appendix C. Rheological models from Akaike criterion standpoint

To further expand the assessment of the rheological models' performance in describing the experimental measurements in this study, the Akaike information criterion (AIC) is also utilized for each of three models. Mathematically speaking, increasing the number of parameters within models allows more flexibility in capturing a given set of data, however it results in increasing the complexity of the model and the possibility of overfitting the data. The AIC is a measure of comparing models' performance in predicting a given series of measured data, i.e. SWS in this study, jointly in terms of a model's predictive power as well as the number of associated parameters each model employs [27]. Therefore, there is a trade-off between the model's complexity and its ability to capture data. The AIC parameter is calculated from equation C.1, using the least squares fitting approach.

$$AIC = N \cdot Ln\left(\frac{RSS}{N}\right) + 2 \cdot K \tag{C.1}$$

In this equation, N is the number of measurements, K is the number of parameters within each model plus 1 (to account for the error), and RSS is the residual sum of squares comparing the model predictions against measurements. Evaluating the AIC parameter for each of the three rheological models in this study, i.e. the KV, SLS, and KVFD models, the model with the lowest value of AIC is the model representing the best trade-off. Table C.1 summaries the results of AICs for the three models. It is noted that the KVFD model has the lowest AIC (negative because of the natural log of a small argument) and therefore, is the most appropriate model based on this criterion, consistent with the results obtained from approach A and B.

Table C.1
The Akaike information criterion for the three rheological models in capturing the experimental SWS measurements.

Rheological Model:	AIC
KV model	-24.4
SLS Model	-36.0
KVFD Model	-48.1

Appendix D. Insight into the spring-pot model for tissues

We simply assume that a real macroscopic block of tissues is comprised of multiple components over different scales, from small to large and with a range of individual time constants. In this case, if each component contributes to the stress relaxation at their respective time constant τ_n where $1 \le n \le N$, then the simplest model for this looks like a parallel set of Maxwell elements as shown in Fig. D.1.

This arrangement of multiple parallel elements and an optional single spring element is the generalized Maxwell-Weichert model [51] and has longstanding history as a useful multi-scale, multi-time constant model. We can write the stress relaxation solution for N Maxwell elements simply as a Prony series [60]

$$\sigma_{SR}(t) = \sum_{n=1}^{N} E_n e^{\frac{-t}{\tau_n}} \tag{D.1}$$

where E_n are the relative stiffness of the components with characteristic relaxation time constant $\tau_n = \frac{\eta_n}{E_n}$. Next, if we allow a continuous distribution of time constants τ, the summation becomes an integral and $A(\tau)$ is traditionally called the relaxation spectrum

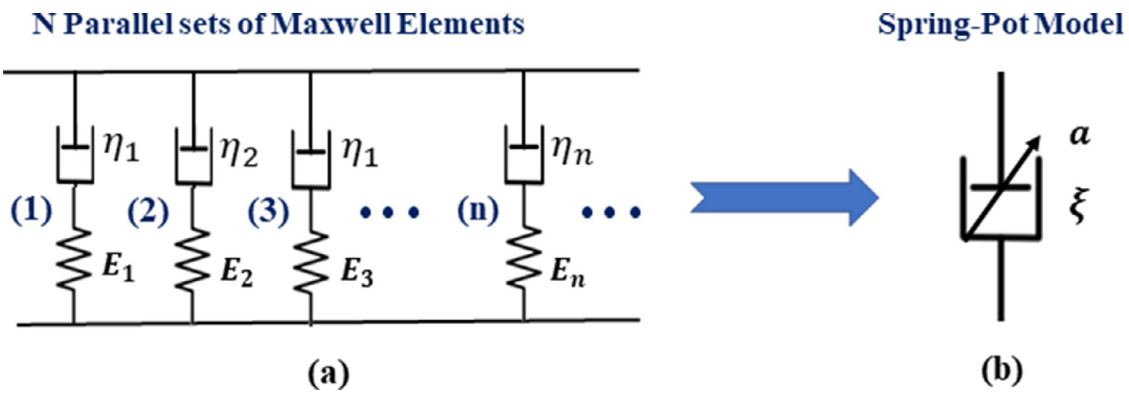

Fig. D.1. **(a)** Parallel Maxwell elements. (b) 2-element spring-pot model.

[51]. Given a material's $A(\tau)$, we can write:

$$\sigma_{SR}(t) = \int_0^\infty A(\tau) e^{-\frac{t}{\tau}} d\tau \tag{D.2}$$

Now let us assume the relaxation spectrum is a power-law distribution characterized by parameter b where $b > 1$.:

$$A(\tau) = A_0 \tau^{-b}; \quad 1 < b < 2 \tag{D.3}$$

A strong rationale for introducing this function is that the power law distribution is frequently found to describe multi-scale systems in nature and biology [52,53]. For example, Carstensen found that a relaxation function of approximately 1/frequency provides the best fit to ultrasound absorption in protein solutions (see his Fig. 8 in Carstensen and Schwan [52]).

Substituting equation (D.2) into equation (D.3) yields precisely the spring-pot, with the associated time and frequency domain behavior similar to the form shown in **Table 1**. In particular, assuming a simple change of variable for the power-law parameter as $b = a + 1$, the stress relaxation will be proportional to $1/t^a$ for $a > 0$ and $t > 0$, and the complex modulus $\hat{E}(\omega)$ will be a power-law of the form proportional to ω^a where $a > 0$. Further details of this result can be found in [26,54]. In summary, the 2-parameter spring pot is a natural consequence of having a multi-scale distribution of relaxation mechanisms which appear to be present in tissues.

References

[1] J. Ormachea, K.J. Parker, Elastography imaging: the 30 year perspective, Phys. Med. Biol. 65 (24) (2020) 24TR06.
[2] H. Li, G. Flé, M. Bhatt, Z. Qu, S. Ghazavi, L. Yazdani, G. Bosio, I. Rafati, G. Cloutier, Viscoelasticity imaging of biological tissues and single cells using shear wave propagation, Front. Phys. 9 (2021) 350.
[3] R.G. Barr, G. Ferraioli, M.L. Palmeri, Z.D. Goodman, G. Garcia-Tsao, J. Rubin, B. Garra, R.P. Myers, S.R. Wilson, D. Rubens, Elastography assessment of liver fibrosis: society of radiologists in ultrasound consensus conference statement, Radiology 276 (3) (2015) 845–861.
[4] A.K. Sharma, J. Reis, D.C. Oppenheimer, D.J. Rubens, J. Ormachea, Z. Hah, K.J. Parker, Attenuation of shear waves in normal and steatotic livers, Ultrasound Med. Biol. 45 (4) (2019) 895–901.
[5] H. Tzschätzsch, S. Ipek-Ugay, M.N. Trong, J. Guo, J. Eggers, E. Gentz, T. Fischer, M. Schultz, J. Braun, I. Sack, Multifrequency time-harmonic elastography for the measurement of liver viscoelasticity in large tissue windows, Ultrasound Med. Biol. 41 (3) (2015) 724–733.
[6] C.T. Barry, B. Mills, Z. Hah, R.A. Mooney, C.K. Ryan, D.J. Rubens, K.J. Parker, Shear wave dispersion measures liver steatosis, Ultrasound Med. Biol. 38 (2) (2012) 175–182.
[7] K.R. Nightingale, N.C. Rouze, S.J. Rosenzweig, M.H. Wang, M.F. Abdelmalek, C.D. Guy, M.L. Palmeri, Derivation and analysis of viscoelastic properties in human liver: impact of frequency on fibrosis and steatosis staging, IEEE Trans. Ultrason. Ferroelectr. Freq. Control 62 (1) (2015) 165–175.
[8] M. Muller, J.L. Gennisson, T. Deffieux, M. Tanter, M. Fink, Quantitative viscoelasticity mapping of human liver using supersonic shear imaging: preliminary *in vivo* feasability study, Ultrasound Med. Biol. 35 (2) (2009) 219–229.
[9] I.H. Faris, J. Melchor, A. Callejas, J. Torres, G. Rus, Viscoelastic biomarkers of *ex vivo* liver samples via torsional wave elastography, Diagnostics 10 (2) (2020) 111.
[10] V. Kumar, M. Denis, A. Gregory, M. Bayat, M. Mehrmohammadi, R. Fazzio, M. Fatemi, A. Alizad, Viscoelastic parameters as discriminators of breast masses: initial human study results, PLoS One 13 (10) (2018) e0205717.
[11] A. Nabavizadeh, M. Bayat, V. Kumar, A. Gregory, J. Webb, A. Alizad, M. Fatemi, Viscoelastic biomarker for differentiation of benign and malignant breast lesion in ultra-low frequency range, Sci. Rep. 9 (1) (2019) 1–12.
[12] M. Zhang, P. Nigwekar, B. Castaneda, K. Hoyt, J.V. Joseph, A. di Sant'Agnese, E.M. Messing, J.G. Strang, D.J. Rubens, K.J. Parker, Quantitative characterization of viscoelastic properties of human prostate correlated with histology, Ultrasound Med. Biol. 34 (7) (2008) 1033–1042.
[13] M.W. Urban, A.D. Rule, T.D. Atwell, S. Chen, Novel uses of ultrasound to assess kidney mechanical properties, Kidney 2 (9) (2021) 1531–1539.
[14] C. Amador, M.W. Urban, S. Chen, J.F. Greenleaf, Shearwave dispersion ultrasound vibrometry (SDUV) on swine kidney, IEEE Trans. Ultrason. Ferroelectr. Freq. Control 58 (12) (2011) 2608–2619.
[15] H. Herthum, S.C. Dempsey, A. Samani, F. Schrank, M. Shahryari, C. Warmuth, H. Tzschätzsch, J. Braun, I. Sack, Superviscous properties of the *in vivo* brain at large scales, Acta Biomater. 121 (2021) 393–404.
[16] R.G. Gary, F. Zvietcovich, J.P. Rolland, H. Mestre, M. Giannetto, M. Nedergaard, K.J. Parker, A preliminary study on using reverberant shear wave fields in optical coherence elastography to examine mice brain *ex vivo*, Optical Elastography and Tissue Biomechanics VI, Int. Soc. Opt. Photonics (2019) p. 108801D.
[17] G. Franchini, I.D. Breslavsky, G.A. Holzapfel, M. Amabili, Viscoelastic characterization of human descending thoracic aortas under cyclic load, Acta Biomater. 130 (2021) 291–307.
[18] M. Amabili, P. Balasubramanian, I. Breslavsky, Anisotropic fractional viscoelastic constitutive models for human descending thoracic aortas, J. Mech. Behav. Biomed. Mater. 99 (2019) 186–197.
[19] J. Ormachea, K.J. Parker, Comprehensive viscoelastic characterization of tissues and the inter-relationship of shear wave (group and phase) velocity, attenuation and dispersion, Ultrasound Med. Biol. 46 (12) (2020) 3448–3459.
[20] P. Kijanka, M.W. Urban, Dispersion curve calculation in viscoelastic tissue-mimicking materials using non-parametric, parametric, and high-resolution methods, Ultrasonics 109 (2021) 106257.
[21] S. Bernard, S. Kazemirad, G. Cloutier, A frequency-shift method to measure shear-wave attenuation in soft tissues, IEEE Trans. Ultrason. Ferroelectr. Freq. Control 64 (3) (2016) 514–524.
[22] A. Callejas, A. Gomez, I.H. Faris, J. Melchor, G. Rus, Kelvin–voigt parameters reconstruction of cervical tissue-mimicking phantoms using torsional wave elastography, Sensors 19 (15) (2019) 3281.
[23] A. Callejas, J. Melchor, I.H. Faris, G. Rus, Viscoelastic model characterization of human cervical tissue by torsional waves, J. Mech. Behav. Biomed. Mater. 115 (2021) 104261.
[24] L. Peralta, G. Rus, N. Bochud, F. Molina, Assessing viscoelasticity of shear wave propagation in cervical tissue by multiscale computational simulation, J. Biomech. 48 (9) (2015) 1549–1556.
[25] A. Gomez, G. Rus, N. Saffari, Wave propagation in a fractional viscoelastic tissue model: application to transluminal procedures, Sensors 21 (8) (2021) 2778.
[26] K. Parker, T. Szabo, S. Holm, Towards a consensus on rheological models for elastography in soft tissues, Phys. Med. Biol. 64 (21) (2019) 215012.
[27] S. Portet, A primer on model selection using the Akaike Information Criterion, Infect. Dis. Modell. 5 (2020) 111–128.
[28] S.S. Poul, J. Ormachea, S.J. Hollenbach, K.J. Parker, Validations of the microchannel flow model for characterizing vascularized tissues, Fluids 5 (4) (2020) 228.

[29] A. Freed, K. Diethelm, Fractional calculus in biomechanics: a 3D viscoelastic model using regularized fractional derivative kernels with application to the human calcaneal fat pad, Biomech. Model. Mechanobiol. 5 (4) (2006) 203–215.
[30] C. Wex, C. Bruns, A. Stoll, Fractional kelvin-voight model for liver tissue in the frequency and time domain, Scottish Journal of Arts, Social Sciences and Scientific Studies 11(2) (2014) 69-78.
[31] S. Näsholm, S. Holm, On a fractional Zener elastic wave equation, Fract. Calc. Appl. Anal. 16 (1) (2013) 26–50.
[32] M. Caputo, J.M. Carcione, F. Cavallini, Wave simulation in biologic media based on the Kelvin-Voigt fractional-derivative stress-strain relation, Ultrasound Med. Biol. 37 (6) (2011) 996–1004.
[33] M. Zhang, B. Castaneda, Z. Wu, P. Nigwekar, J.V. Joseph, D.J. Rubens, K.J. Parker, Congruence of imaging estimators and mechanical measurements of viscoelastic properties of soft tissues, Ultrasound Med. Biol. 33 (10) (2007) 1617–1631.
[34] M.Z. Kiss, T. Varghese, T.J. Hall, Viscoelastic characterization of *in vitro* canine tissue, Phys. Med. Biol. 49 (18) (2004) 4207.
[35] R.L. Magin, Fractional calculus in bioengineering, Begell House Redding, 2006.
[36] S.S. Poul, K.J. Parker, Fat and fibrosis as confounding cofactors in viscoelastic measurements of the liver, Phys. Med. Biol. 66 (4) (2021) 045024.
[37] V. Vincek, M. Nassiri, J. Knowles, M. Nadji, A.R. Morales, Preservation of tissue RNA in normal saline, Lab. Invest. 83 (1) (2003) 137–138.
[38] T. Loupas, R.B. Peterson, R.W. Gill, Experimental evaluation of velocity and power estimation for ultrasound blood flow imaging, by means of a two-dimensional autocorrelation approach, IEEE Trans. Ultrason. Ferroelectr. Freq. Control 42 (4) (1995) 689–699.
[39] J. Ormachea, K. Parker, Reverberant shear wave phase gradients for elastography, Phys. Med. Biol. 66 (17) (2021) 175001.
[40] F. Zvietcovich, P. Pongchalee, P. Meemon, J.P. Rolland, K.J. Parker, Reverberant 3D optical coherence elastography maps the elasticity of individual corneal layers, Nat. Commun. 10 (1) (2019) 1–13.
[41] G. Mattei, A. Ahluwalia, Sample, testing and analysis variables affecting liver mechanical properties: a review, Acta Biomater. 45 (2016) 60–71.
[42] W.C. Yeh, P.C. Li, Y.M. Jeng, H.C. Hsu, P.L. Kuo, M.L. Li, P.M. Yang, P.H. Lee, Elastic modulus measurements of human liver and correlation with pathology, Ultrasound Med. Biol. 28 (4) (2002) 467–474.
[43] K. Tan, S. Cheng, L. Jugé, L.E. Bilston, Characterising soft tissues under large amplitude oscillatory shear and combined loading, J. Biomech. 46 (6) (2013) 1060–1066.
[44] S. Chen, M.W. Urban, C. Pislaru, R. Kinnick, J.F. Greenleaf, Liver elasticity and viscosity quantification using shearwave dispersion ultrasound vibrometry (SDUV), 2009 Annual International Conference of the IEEE Engineering in Medicine and Biology Society, IEEE, 2009, pp. 2252-2255.
[45] D. Klatt, U. Hamhaber, P. Asbach, J. Braun, I. Sack, Noninvasive assessment of the rheological behavior of human organs using multifrequency MR elastography: a study of brain and liver viscoelasticity, Phys. Med. Biol. 52 (24) (2007) 7281.
[46] B. Suki, A.L. Barabasi, K.R. Lutchen, Lung tissue viscoelasticity: a mathematical framework and its molecular basis, J. Appl. Physiol. 76 (6) (1994) 2749–2759.
[47] M.E. Newman, Power laws, Pareto distributions and Zipf's law, Contemp. Phys. 46 (5) (2005) 323–351.
[48] K.J. Parker, Power laws prevail in ultrasound-tissue interactions, Phys. Med. Biol. 67 (9) (2022) 09TR02.
[49] W. Zhang, A. Capilnasiu, D. Nordsletten, Comparative analysis of nonlinear viscoelastic models across common biomechanical experiments, J. Elast. 145 (1) (2021) 117–152.
[50] A. Capilnasiu, L. Bilston, R. Sinkus, D. Nordsletten, Nonlinear viscoelastic constitutive model for bovine liver tissue, Biomech. Model. Mechanobiol. 19 (5) (2020) 1641–1662.
[51] Y.C. Fung, Biomechanics: mechanical properties of living tissues, Chapter 2, Springer-Verlag, New York, 1981.
[52] E.L. Carstensen, H.P. Schwan, Acoustic properties of hemoglobin solutions, J. Acoust. Soc. Am. 31 (3) (1959) 305–311.
[53] G.B. West, J.H. Brown, B.J. Enquist, The fourth dimension of life: fractal geometry and allometric scaling of organisms, Science 284 (5420) (1999) 1677–1679.
[54] K. Parker, A microchannel flow model for soft tissue elasticity, Phys. Med. Biol. 59 (15) (2014) 4443.
[55] M. Amabili, P. Balasubramanian, I. Bozzo, I.D. Breslavsky, G. Ferrari, Layer-specific hyperelastic and viscoelastic characterization of human descending thoracic aortas, J. Mech. Behav. Biomed. Mater. 99 (2019) 27–46.
[56] M. Amabili, P. Balasubramanian, I. Bozzo, I.D. Breslavsky, G. Ferrari, G. Franchini, F. Giovanniello, C. Pogue, Nonlinear dynamics of human aortas for material characterization, Phys. Rev. X 10 (1) (2020) 011015.
[57] D. Nordsletten, A. Capilnasiu, W. Zhang, A. Wittgenstein, M. Hadjicharalambous, G. Sommer, R. Sinkus, G.A. Holzapfel, A viscoelastic model for human myocardium, Acta Biomater. 135 (2021) 441–457.
[58] G. Rus, I.H. Faris, J. Torres, A. Callejas, J. Melchor, Why are viscosity and nonlinearity bound to make an impact in clinical elastographic diagnosis? Sensors 20 (8) (2020) 2379.
[59] J. Ormachea, K.J. Parker, R.G. Barr, An initial study of complete 2D shear wave dispersion images using a reverberant shear wave field, Phys. Med. Biol. 64 (14) (2019) 145009.
[60] D. Jalocha, A. Constantinescu, R. Neviere, Revisiting the identification of generalized Maxwell models from experimental results, Int. J. Solids Struct. 67 (2015) 169–181.